Available online at www.sciencedirect.com
ScienceDirect
Aerosol Science 39 (2008) 488–499
Journal of Aerosol Science
www.elsevier.com/locate/jaerosci

Experimental study of filtration efficiency of nanoparticles below 20 nm at elevated temperatures

W.G. Shin[a], G.W. Mulholland[b], S.C. Kim[a], D.Y.H. Pui[a,*]

[a] *Department of Mechanical Engineering, The University of Minnesota, Minneapolis 55455, USA*
[b] *Department of Mechanical Engineering, The University of Maryland, College Park, USA*

Received 10 September 2007; received in revised form 14 January 2008; accepted 30 January 2008

Abstract

This paper reports the measurements of the single fiber efficiency for a screen mesh at elevated temperatures up to 500 K for silver nanoparticles in the size range from 3 to 20 nm. Thermal rebound of particles from a filter surface is predicted to occur at 500 K for 3 nm diameter particles based on a theory by Wang and Kasper [(1991). Filtration efficiency of nanometer-size aerosol particles. *Journal of Aerosol Science*, *22*, 31–41]; however, rebound was not detected in our study. A small change in the single fiber efficiency with temperature was observed for a fixed mass flow as is predicted by classical filtration theory. The measured increase of 8% ± 5% for particles of size 3, 4, and 5 nm is less than the 19% predicted by classical filtration theory. Measurements of particle penetration at a temperature of about 600 K were not possible because of particle production within the filter/holder.

Keywords: Filtration efficiency; Elevated temperature; Nanoparticle; Thermal rebound

1. Introduction

Nanotechnology offers great opportunities for new and improved nanostructured, functionalized materials and devices. However, nanoparticle inhalation may cause negative health effects at the point of deposition or may be transmitted to other organs (Kreyling et al., 2002; Oberdorster, Gelein, Ferin, & Weiss, 1995).

Filtration has been widely used to protect individuals from the inhalation of toxic particulate. Recent studies have focused on measuring the filtration efficiency for nanosize particles at room temperature (Heim, Mullins, Wild, Meyer, & Kasper, 2005; Kim & Okuyama, 2006; Kim, Harrington, & Pui, 2007; Wang, Chen, & Pui, 2007). Such studies are needed to assess the effectiveness of filtration for removing nanosize particles. Nanoparticles are believed to be collected with increasing efficiency with decreasing particle size by Brownian deposition. This was demonstrated by several recent papers under room temperature conditions (Heim et al., 2005; Kim et al., 2007). Heim et al. (2005) found that even for particle sizes as small as 2.5 nm there was no measurable deviation from the classical single fiber efficiency theory by Cheng and Yeh (1980). Heim, Mullins, and Kasper (2006) showed that the measurement anomaly which Ichitsubo, Hashimoto, Alonso, and Kousaka (1996) misinterpreted as thermal rebound, and reanalyzed the data to show that thermal rebound does not occur down to 1.33 nm. At smaller sizes in the range of 1–2 nm, Kim and Okuyama

* Corresponding author. Tel.: +1 6126252537; fax: +1 6126256069.
E-mail address: dyhpui@umn.edu (D.Y.H. Pui).

0021-8502/$ - see front matter © 2008 Elsevier Ltd. All rights reserved.
doi:10.1016/j.jaerosci.2008.01.006

(2006) found that the filter efficiency decreased rather than continuing to increase. This is a direct observation of particle bounce. In their study, the filtration efficiency was measured for two types of glass fibrous filters using a particle size magnifier at room temperature conditions.

This effect of decreasing efficiency for nanoparticles is consistent with the theory of Wang and Kasper (1991). They predict that thermal impact velocity of a particle will exceed the critical sticking velocity at some point below 10 nm and that the particle will bounce off filter surfaces due to their large thermal velocity. This process will result in additional penetration of the particle through the filter. However, the prediction of a specific onset particle diameter for thermal rebound based on their model is difficult because of lack of information regarding the Hamaker constant and specific adhesion energy constant needed in their model.

At the elevated temperatures, nanoparticles in the small size range below 10 nm will be more likely to bounce off the surface of the filter media compared to room temperature. This is, in part, because of the increased speed of the nanoparticle.

There are important applications of filtration at elevated temperatures including the effluent from biomass combustion, waste incineration processes, and diesel engines. Often filtration is used to reduce particulate emissions to meet environmental regulations. Ceramic and metallic media have been used for particle filtration for hot process gas rather than cyclones and electrostatic precipitators. Cyclones can withstand high temperatures and are relatively cheap and easy to operate, but their particle collection efficiency is low for particles below 10 μm. Electrostatic precipitators are very efficient for small particles and can operate at high temperature, but they are expensive even for small scale plants. Previous work on high temperature filtration has been mainly focused on the micrometer size range (Hemmer, Hoff, & Kasper, 2003; Freistas, Goncalves, Innocentini, Mullins, & Coury, 2006). Therefore, it is important to investigate nanoparticle filtration at elevated temperatures.

In this study, a high temperature filtration test system has been developed to characterize single fiber collection efficiency for monodisperse particles over the size range from 3 to 20 nm. Key design challenges are to form a good seal for the filters at elevated temperatures, to compensate for thermophoretic deposition in the sampling line, and to avoid the generation of nanoparticles from the heated filter/filterholder. Silver particles were used as the test aerosol. The singly charged particles were neutralized to avoid electrostatic deposition. A stainless steel screen mesh was used as the test filter to determine whether the classical single fiber efficiency model (Cheng & Yeh, 1980) can be applied to filtration process at elevated temperatures. There is also interest in determining whether thermal rebound occurs as a result of increasing the thermal speed of the particles by about 30%. Our experimental results will be compared with the predictions of the Wang–Kasper theory for the change in particle penetration for a 200 °C temperature increase.

2. Theory

From conservation of mass, penetration of particles through a filter element is given by (Dorman, 1966, chap. 8)

$$P = \exp(-nSE_s), \tag{1}$$

where n is the number of layers, S is screen parameter, and E_s is single fiber collection efficiency. The screen parameter (S) of the screen type mesh is defined by (Dorman, 1966, chap. 8)

$$S = \frac{4\alpha h}{\pi(1-\alpha)d_f}, \tag{2}$$

where α, h, and d_f are the solid volume fraction, thickness, and fiber diameter of screen, respectively. The screen parameter represents the fractional capture per unit thickness (h) divided by single fiber efficiency. The solid volume fraction (α) is estimated by measuring the volume of solid and total volume of screen:

$$\alpha = \frac{4m_s}{\pi d_s^2 h \rho_s}, \tag{3}$$

where m_s, d_s, and ρ_s are mass, diameter, and density of screen, respectively. For multiple layers of screens, different rows will be randomly oriented and are described by fan model filtration theory (Kirsch & Stechkina, 1978, Chap. 4). In the continuum flow regime for the fiber, the single fiber efficiency for diffusive deposition in filter elements of different geometrical arrangements was obtained by Kirsch and Stechkina (1978, chap. 4)

$$E_s = 2.7\,Pe^{-2/3} \quad \text{for the fan model.} \tag{4}$$

The quantity Pe is the Peclet number defined by:

$$Pe = \frac{d_f U}{D}, \tag{5}$$

where U is face velocity and D is diffusion coefficient. The quantity D is determined by Stokes–Einstein equation:

$$D = \frac{kTC}{3\pi\mu d}, \tag{6}$$

where k is Boltzmann's constant, T is absolute temperature, C is slip correction factor, μ is viscosity, and d is particle diameter.

The viscosity as a function of absolute temperature is obtained using the Sutherland formula as discussed by Allen and Rabbe (1982):

$$\mu_T = \mu_{23}\left(\frac{T}{T_0}\right)^{1.5}\left(\frac{T_0 + 110.4}{T + 110.4}\right), \tag{7}$$

where μ_{23} is the reference viscosity at 296.15 K.

The slip correction factor C is expressed as

$$C = 1 + \frac{\lambda}{d}\left[2.34 + 1.05\exp\left(-0.39\frac{d}{\lambda}\right)\right], \tag{8}$$

where λ is the mean free path. The mean free path as a function of temperature and pressure is expressed by Willeke's (1976) relation:

$$\lambda = \lambda_0\left(\frac{T}{T_0}\right)\left(\frac{P_0}{P}\right)\left(\frac{1 + 110.4/T_0}{1 + 110.4/T}\right), \tag{9}$$

where λ_0 is the 67.3 nm for air at T_0, P_0, T_0 the reference temperature, 296.15 K, P_0 the reference pressure, 101.35 kPa, T the air temperature in the filter upstream inside the filter holder, and P the air pressure in the filter upstream inside the filter holder.

The diffusion coefficient (D) has a dependence on $T^{3/2}$ as a result of the $T^{1/2}$ dependence of the viscosity and the T dependence of the slip correction factor for the free molecular regime. Therefore, from Eq. (4), the single fiber efficiency (E_s) by diffusion for constant face velocity is

$$E_s \sim T. \tag{10}$$

A sensitive measure of the temperature dependence of E_s is the ratio E_s/T. In Fig. 1 this ratio normalized by its value at $T = 296$ K is plotted versus temperature for 3, 4, 9, and 20 nm particle diameters with a fixed face velocity of 5 cm/s and wire diameter of 90 μm. The plot indicates that this ratio decreases by less than 2% for temperatures up to 500 K. This shows that Eq. (10) is a good estimate of the temperature dependence over the temperature and particle size range of interest.

In the experiments, the face velocity is proportional to absolute temperature, because there is a constant mass flow into the filter holder. As a result, the temperature dependence of single fiber efficiency is reduced according to the equation below:

$$E_s \sim T^{1/3}. \tag{11}$$

Wang and Kasper (1991) predict that as the particle size decreases below a critical size, a fraction of particles bounce from the filter surface. A key quantity in computing collision effectiveness, R, is given by

$$R = \frac{V_{th}}{V_{cr}} = \frac{0.28(kT)^{1/2}}{(K_p + K_s)^{1/3}\sigma_{p,s}^{5/6} D_p^{2/3}}, \tag{12}$$

where V_{th} is mean thermal velocity of particle, V_{cr} is critical velocity for bounce, $\sigma_{p,s}$ is specific adhesion energy at interfacial contact, and K_p and K_s are mechanical constants of particle and substrate. The adhesion efficiency ε is a

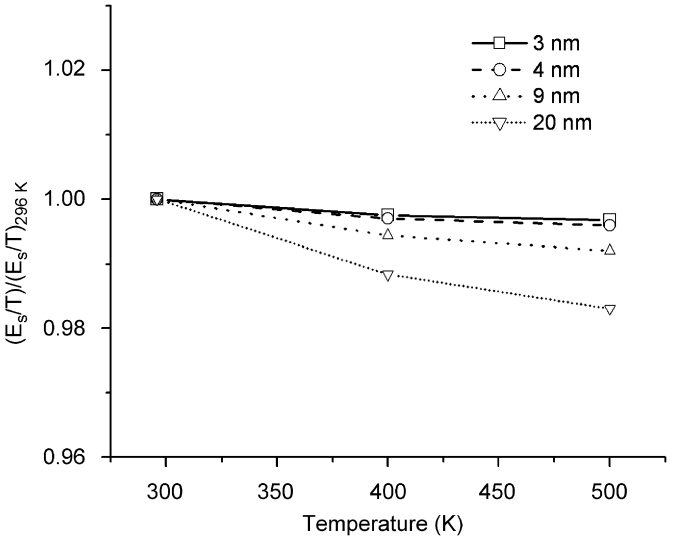

Fig. 1. Dependence of single fiber efficiency on temperature for 3, 4, 9, and 20 nm.

function of R and decreases as R^3 for $R > 2$. The temperature dependence for $\sigma_{p,s}$ is assumed to be the same as the surface tension of a liquid:

$$\sigma_{p,s} \sim T^{-1}. \tag{13}$$

Substituting Eq. (13) into Eq. (12), we obtain the following expression for the dependence of R on T and D_p:

$$R \sim \frac{T^{4/3}}{D_p^{2/3}}. \tag{14}$$

A temperature increase from about 300 to 500 K or a particle size decrease from 3 to 1 nm both increases R by about a factor of 2. This result indicates that a 200 K temperature increase would result in particle bounce. Thus, by doing filtration experiments at elevated temperatures, the Wang–Kasper theory can be tested.

3. Experimental methods

The experimental setup shown in Fig. 2 consists of: (1) Ag particle generation section, (2) monodisperse particle classification section, and (3) high temperature filtration efficiency measurement section. A test facility was constructed to generate Ag nanoparticles with an electrical mobility size range from 3 to 20 nm. Ag wire (purity level 99.9%) was placed in a ceramic boat, which, in turn, was placed inside a quartz tube. As shown in Fig. 2, the quartz tube is heated by an electric tube furnace. Nitrogen with a flow rate of 3.0 L/min was used as a carrier gas passing through the quartz tube. The flow rate of the carrier gas was regulated by a rotameter and monitored by a TSI mass flow meter. Silver was vaporized in the electric furnace followed by particle formation and growth by condensation and coagulation. The setup of silver generation system used in this experiment is very similar to that in our previous paper (Shin, Pui, Fissan, Neumann, & Trampe, 2007). In the size range up to 20 nm, the silver particles generated from the electric furnace are single homogenous spheres (Scheibel & Porstendorfer, 1983).

Silver nanoparticles are size classified by a Nano-DMA (DMA-Model 3085, TSI, Inc.). First a bipolar charge distribution of the aerosol is obtained by passage through a tube containing Po-210, an α emitter. Then a monodisperse fraction of charged particles is selected with the Nano-DMA. The sheath flow rate and aerosol flow rate for Nano-DMA are 10 L/min and 1 L/min, respectively. After exiting the Nano-DMA, the silver nanoparticles are passed through a second bipolar charger, which neutralizes over 95% of the charged particles. Make-up air is introduced at the inlet of the filter holder. The face velocity is controlled by a critical orifice downstream of filter holder. The flow through the filter holder is laminar with a maximum Reynolds number based on the inner diameter of filter holder of 665 at

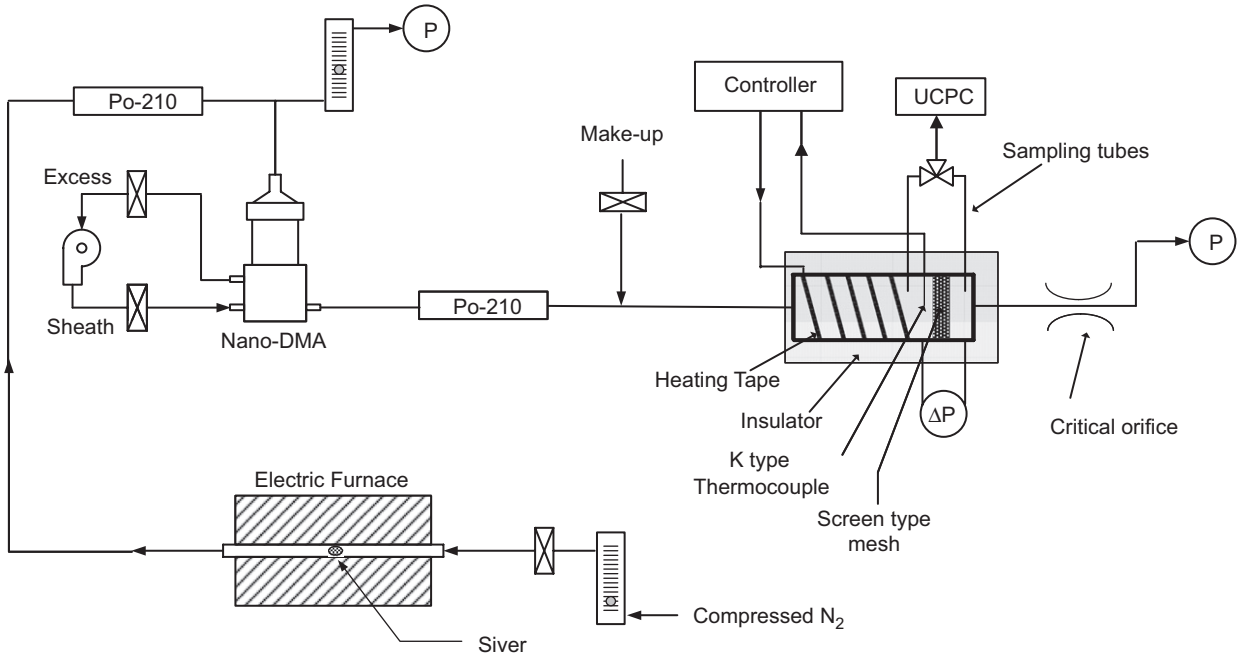

Fig. 2. Schematic diagram of experimental setup.

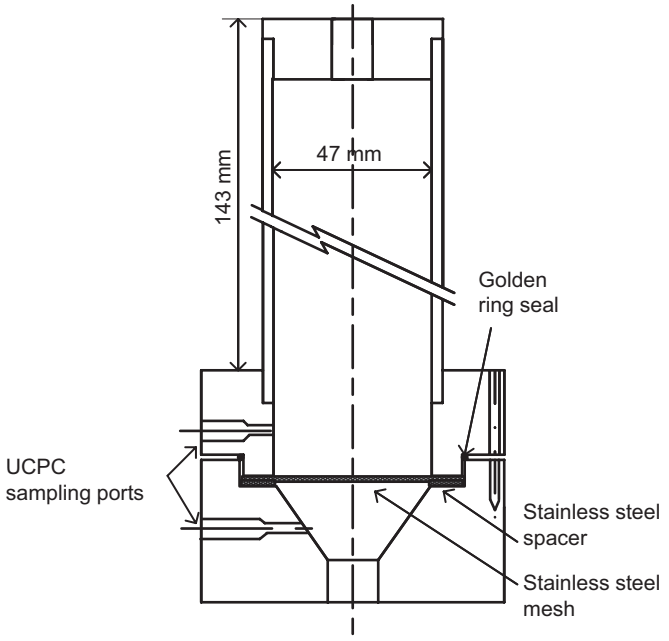

Fig. 3. Schematic diagram of filter holder: As the two parts of the filter holder are bolted together, the golden ring seal is compressed preventing leakage from the outside and the stainless steel mesh is also compressed preventing leakage around the edge of the mesh.

$U = 9.5\,\mathrm{cm/s}$ and 296 K. In our experiments, the initial (upstream) number concentration of Ag particles varied with particle size. For the 3 nm size, which has the smallest initial number concentration of Ag particles, the downstream concentration is $644\,\mathrm{cm}^{-3}$. For the other sizes, the concentrations were higher than that of 3 nm.

Fig. 3 shows a schematic diagram of the filter holder used in this study. The filter holder consists of two cylindrical chambers made of stainless steel. The test filter was tightly fixed against a stainless steel spacer between two chambers

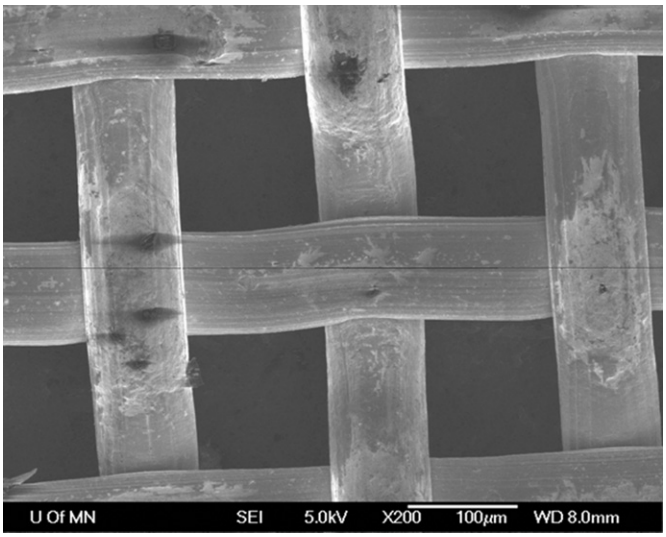

Fig. 4. SEM image of stainless steel screen mesh.

by three stainless bolts with a low thermal expansion coefficient. In order to avoid out-gassing from plastic materials such as Teflon gaskets, all tubing fittings were welded together, and a ring seal made of gold was used to prevent leakage at the interface of two chambers. Heating tape (Model STH051-040, OMEGA, Inc.) was wrapped around the long entrance part (143 mm) of the filter holder to heat up the air flow laden with silver nanoparticles. The temperature of flow inside the filter holder was fixed by a temperature controller (Model CN2110, OMEGA, Inc.) with temperature measurement using a K type thermocouple (Model GKMQSS-062, OMEGA, Inc.). The thermocouple was located at the center of the cylindrical chamber just before the surface of the filter. The whole outer surface of the filter holder was insulated to ensure isothermal conditions. Results of heat transfer calculations for the temperature distribution are given in the next section of the paper.

The number concentrations of particles were measured for 1 min both upstream and downstream using a UCPC, a condensation particle counter capable of detecting particles as small as 3 nm (CPC Model 3025, TSI, Inc.). The counting efficiency of TSI CNC 3025 at the size of 3 nm is about 50% based on the specification sheet of the manufacturer, TSI Inc. Similar counting efficiencies were also obtained by Cofer, Anderson, Winstead, and Bagwell (1998) and Heim et al. (2005). Because the efficiency is the same for both the upstream and downstream concentration measurement, the counting efficiency will cancel out when taking the ratio of the two concentrations. The configuration and length of particle sampling lines from both the inlet and outlet of the filter holder to the UCPC were kept identical so that thermophoretic particle loss would be the same in both lines. The upstream and downstream number concentration measurements were repeated 3 times for each test. The standard deviation of the mean penetration divided by mean value is between 0.003 and 0.020.

The test filter was a stainless steel screen mesh (Manufacturer: McMaster-CARR). A coarse screen mesh with relatively low filtration efficiency was selected so there would be an adequate particle number concentration downstream of the filter. An SEM image (Fig. 4) of the screen mesh shows that the wire diameter (d_f) is 90 μm. The assumption of continuous flow around the wires is valid, since the calculated Knudsen number, Kn, 2.76×10^{-3} at 500 K, is much less than 1. As shown in Fig. 4, fibers are woven together in a single layer. The average thickness (h) of the screen mesh is 203 μm and is used for calculating the solid volume fraction using Eq. (3). The solid volume fraction (α) is 0.3105 and the cross-sectional diameter of the screen mesh open to the flow is 47 mm.

When the filter holder is first heated and purged with clean air, particles are generated from inside the filter holder. The generated particles may originate as solid particles from within the filter holder/filter or they may result from the production of condensable vapor from the holder/filter. The chamber was tempered and purged with filtered air at 613 K for several days before performing the measurements at 500 K. The particle concentration versus time is shown in Fig. 5 for a period of 2 h for the filter heated to 613 K. It is seen that the number concentration decreases from about 10^5 cm^{-3} to about 10 cm^{-3}. Even after 48 h the concentration is about 10 cm^{-3}. Thus, filtration experiments were not

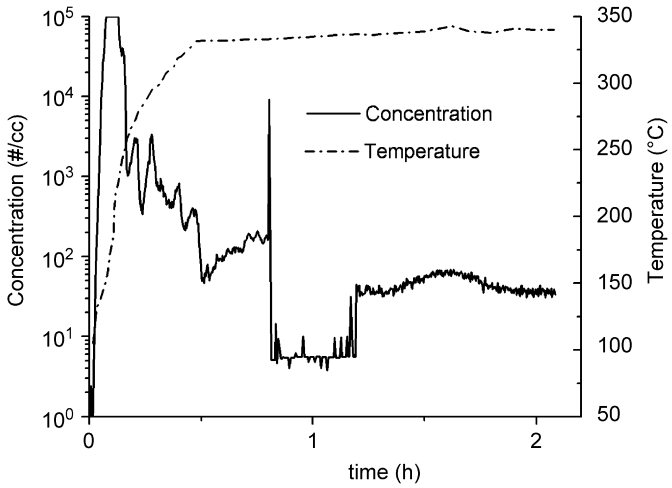

Fig. 5. Profile of particle emission at 340 °C.

possible at 600 K. At 500 K, the highest temperature used, we did not observe particle emission. During the testing of a filter, we passed clean air through the system and did not detect any particles.

4. Results and discussion

Fig. 6a shows the schematic diagram of approximate temperature profile around the filter inside the filter holder. The measured variation of temperature was small in the radial direction as shown in Fig. 6b. The ratio $(T_c - T_w)/(T_c - T_a)$ is about 0.07. The temperature adjacent to the wall (T_w) is a little lower than the temperature at the center (T_c) because the wall near the filter is not heated directly by heating tape. It is heated primarily via conduction from the upstream wall with some heat transport from the flowing gas. While this region is insulated, there are some heat losses through the insulation, the sampling lines, and the exhaust line.

Numerical simulations of the temperature distribution inside the filter holder were carried out using FLUENT. An axisymmetric geometry was used and a k–ε turbulent model was used to describe jet flow from a 10 mm diameter tube into the 47 mm diameter filter holder. The inlet velocity is assumed to be uniform. A constant heat flux is assumed around the long entrance region, and the boundary condition for the walls near the filter is assumed to be adiabatic. In the FLUENT simulations, a porous jump boundary condition was used for modeling the screen mesh. The FLUENT code is then used to solve for the coupled temperature distributions between gas and solid walls. The number of grid cells used for simulation is about 10 000. Steady-state solutions were obtained for both flow and temperature. As shown in Fig. 6b and c, FLUENT result qualitatively shows that the upstream temperature close to the filter surface is uniform.

Thermophoretic velocity (Hinds, 1999) is defined as

$$V_{th} = -\frac{0.55\eta\nabla T}{\rho_g T}. \tag{15}$$

The thermophoretic velocity is about 0.0025 cm/s at 500 K. The temperature gradient was computed using the ratio $(T_c - T_w)/(T_c - T_a)$ obtained from Fig. 6b, which is assumed to be maintained at other temperatures because the filter holder was well insulated. The thermophoretic particle deposition between the two measurement ports of the filter holder can be estimated by the flux change compared to the total flux calculated as

$$\frac{\Delta\text{flux}}{\text{flux}} = \frac{U 2\pi D_{\text{filter holder}} V_{th} t}{U\pi D^2_{\text{filter holder}}}, \tag{16}$$

where $D_{\text{filter holder}}$ is the diameter of the filter holder and t is the time required for the particles to move from the upstream measurement port to the downstream measurement port. The relative flux change is 0.002 for t equal to 1 s

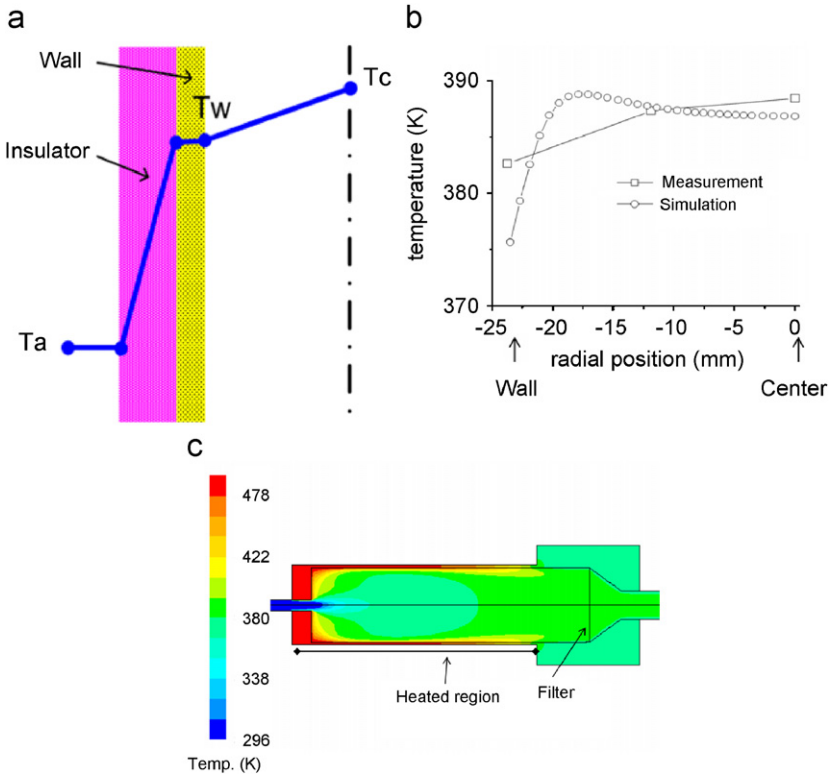

Fig. 6. (a) Schematic diagram of approximate temperature profile around the filter inside filter holder where T_c: temperature at the center, T_w: temperature adjacent to the wall, and T_a: ambient temperature. (b) Comparison of experimental data with simulation result. (c) Simulation result on temperature distribution.

and V_{th} equal to 0.0025 cm/s. Therefore, thermophoretic movement of particles inside the filter holder is insignificant in this study.

The fraction of particles deposited due to thermophoresis f_{th} in the sampling lines going to the UCPC can be estimated using an empirical equation obtained by Mulholland, Henzel, and Babrauskas (1989):

$$f_{th} = (T_h - T_{amb.})/2\,T_h. \tag{17}$$

Using this equation, about 20% of particles will be deposited at T_t equal to 500 K.

Fig. 7 shows the penetration efficiency for a single layer of stainless steel mesh at 296, 400, and 500 K with corresponding values of U equal to 4.17, 5.63, and 7.04 cm/s using neutralized particles. Theory predicts that the penetration decreases as the temperature increases. The temperature effect is greatest for the smallest particle size. The cause of the temperature effect is the temperature dependence of single particle fiber efficiency given in Eq. (11). The difference between experimental and predicted values is typically within 7% with a couple of points deviating by about 10%. The temperature effect ranges from about 1% at 20 nm to about 16% at 3 nm. For the smallest two particle sizes, the penetration data at the highest temperature is clearly less than for the other two temperatures. Below, we consider the effect of temperature on single fiber efficiency for the three smallest particle sizes.

There is no evidence of thermal rebound in these data. Thermal rebound would result in an increase in penetration efficiency with decreasing particle size. This is not seen. Furthermore the data are consistent with the theoretical prediction, which does not include thermal rebound. Therefore, it was found that there is no thermal rebound in the particle size range down to 3 nm at temperatures up to 500 K. Based on the Wang–Kasper theory, a temperature increase from about 300 to 500 K or a particle size decrease from 3 to 1 nm both increases R by about a factor of 2. Kim and Okuyama (2006) observed particle bounce below 2 nm for NaCl particle on fiber filter. Our results do not indicate any particle bounce. Possible reasons for the difference in behavior are that silver particles behave differently than

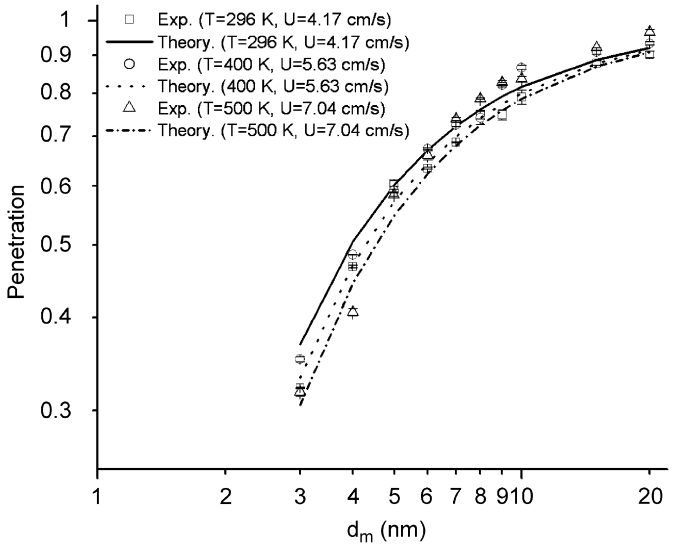

Fig. 7. Penetration efficiency with single layer at 296 K ($U = 4.17$ cm/s), at 400 K ($U = 5.63$ cm/s), and at 500 K ($U = 7.04$ cm/s).

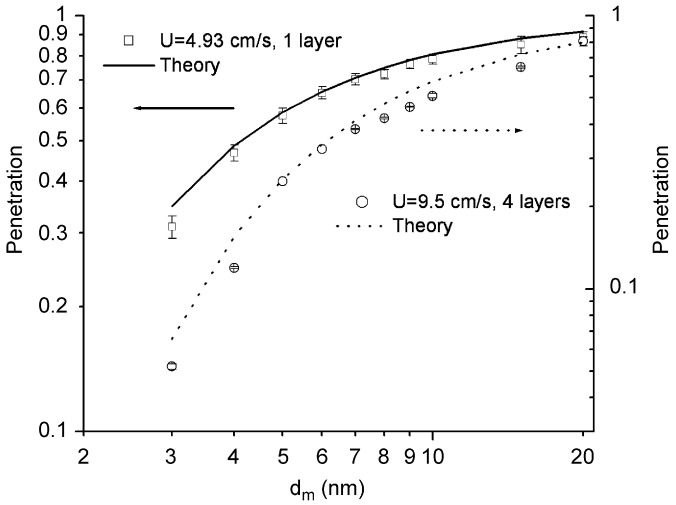

Fig. 8. Penetration efficiency for single layer with $U = 4.93$ cm/s and four layers with $U = 9.5$ cm/s at 350 K.

NaCl or that the assumed temperature dependence of $\sigma_{p,s}$ is incorrect. An extension of our approach might be used to characterize the effect of temperatures on the particle/surface adhesion. That is, if one performs measurements in the small particle size range as a function of temperature and determines the onset of thermal rebound, then the specific adhesion energy at interfacial contact, $\sigma_{p,s}$ can be estimated.

Fig. 8 shows the penetration efficiency of a single layer of stainless steel mesh for U equal to 4.93 cm/s and four layers of stainless steel mesh for U equal to 9.5 cm/s at 350 K. It is seen that the theoretical prediction agrees well with the experimental data for different face velocities and number of layers at the same temperature.

Fig. 9 shows single fiber efficiency for diffusion, E_s, versus Peclet number, Pe, for a single layer of stainless steel mesh tested at 296, 350, 400, and 500 K. The range of Pe is about 5–260 in our experiments. All data sets are collected on the single curve, which is close to classical theory (Cheng & Yeh, 1980). The larger uncertainty for large Peclet number is expected because the penetration is approaching unity.

Fig. 10 shows single fiber efficiency for diffusion for 3, 4, and 5 nm, at several different temperatures. The data set used in Fig. 10 is the same as in Fig. 9. The solid lines indicate the predicted behavior based on Eqs. (4)–(9). All

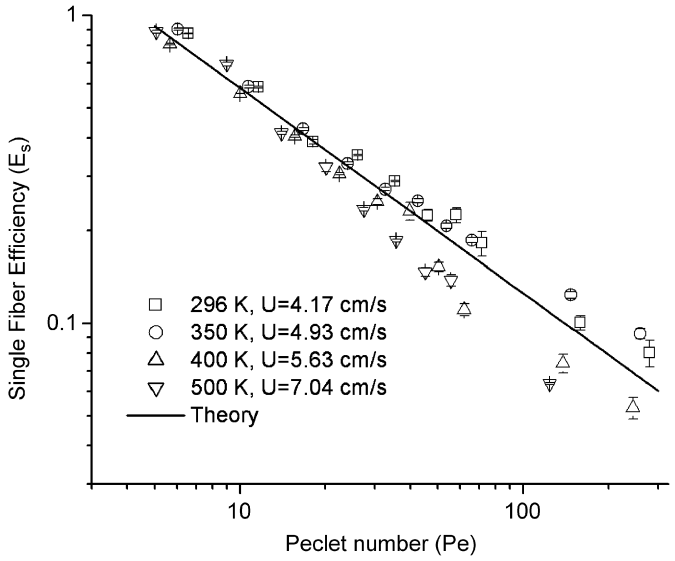

Fig. 9. Single fiber efficiency (E_S) for diffusion versus Peclet number (Pe) at different temperatures.

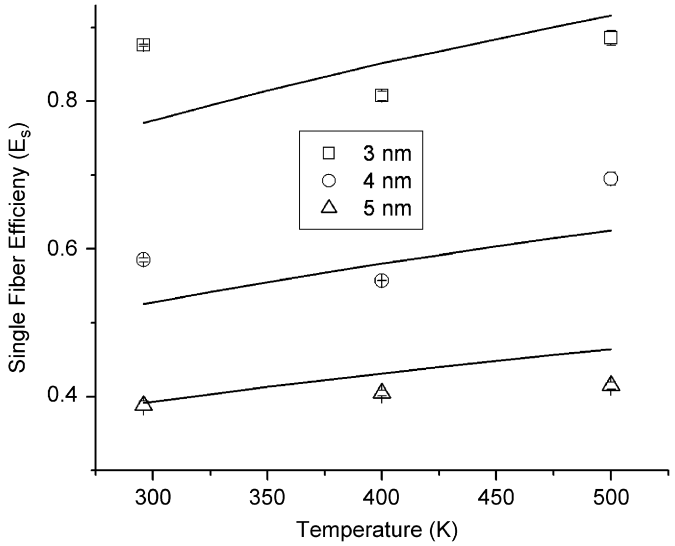

Fig. 10. Comparison of measured and predicted (solid line) single fiber efficiency (E_S) as a function of temperature for a fixed mass flow rate (0.087 g/s).

the measurements are performed for a constant mass flux corresponding to a face velocity of 4.2 cm/s at 296 K. The predicted increase in E_S with a 200 K increase is 19% compared to a measured average increase of 8% ± 5 % based on linear best fits to the data ranging from a 1% increase for the 3 nm data to a 17% increase for the 5 nm data. The data suggests a weaker temperature dependence than predicted by the classical theory; however, the effect is near the uncertainty limits of the measurements. The ±5% uncertainty in the measured increase in E_S is a factor of 2–3 times greater than the uncertainty for the repeat measurements of E_S. This larger than expected value of ±5% suggests there is a small effect that is not controlled in the experiment or is not accounted for in the theory.

Calculated single fiber efficiencies for interception (Lee & Mukund, 2001) and inertial impaction (Yeh & Liu, 1974) are 2.79E − 7 and 2.81E − 7, respectively, for 20 nm at 500 K. Therefore, in this experiment, effects of interception and inertial impaction are negligible.

Our attempt to obtain penetration at 600 K was not successful because of particle production within the filter/holder when particle free air was used. This production persisted over a period of more than two days. Additional work is needed to assess whether these particles are formed from condensing vapors released by the system or whether particles are leaving the surfaces directly.

5. Conclusion

No thermal rebound was detected in the particle size range down to 3 nm and temperatures up to 500 K, even though the mean thermal speed of particles was increased up to 30%. Our experimental results were compared with the predictions of the Wang–Kasper theory for a 200 °C temperature increase. The theory predicts that a temperature increase from about 300 to 500 K or a particle size decrease from 3 to 1 nm both increases the collision effectiveness parameter by about a factor of 2. For sodium chloride particles with a diameter between 1 and 2 nm, particle bounce has been detected. Our results with silver particles do not indicate any particle bounce. The following are two possible reasons for not detecting particle bounce: (1) The difference in adhesion between silver particles/stainless steel filter versus NaCl particle/glass fiber filter (2) An incorrect temperature dependence of $\sigma_{p,s}$ in the Wang–Kasper theory.

Overall, the experimental results agree with the classical theory (Cheng & Yeh, 1980) in the size range 3–20 nm and temperature ranges up to 500 K in terms of the dependence of single particle efficiency E_s on the Peclet number. It was found that the measured E_s increased by about 8% for a 200 K temperature increase at fixed mass flow rate compared to a predicted increase of 19%. The difference between theory and experiment may result from a small effect that is not controlled in the experiment or is not accounted for in the theory. Measurements of filter efficiency at 600 K were not possible because particles were emitted from the filtration system even after more than two days.

Acknowledgments

The authors wish to acknowledge Center for Filtration Research (CFR) at the University of Minnesota for funding this project and University of Minnesota Supercomputing Institute for providing the computation time for this project. Parts of this work were carried out in the University of Minnesota I.T. Characterization Facility, which receives partial support from NSF through the NNIN program. The authors also would like to thank Prof. Thomas Kuehn at the University of Minnesota for his valuable comments on the analysis of heat transfer and an undergraduate research assistant, Yang Yang Bai, for his help in collecting experimental data.

References

Allen, M. D., & Rabbe, O. G. (1982). Re-evaluation of Millikan's oil drop data for the motion of small particles in air. *Journal of Aerosol Science*, *13*, 537–547.

Cheng, Y. S., & Yeh, H. C. (1980). Theory of a screen-type diffusion battery. *Journal of Aerosol Science*, *11*, 313–320.

Cofer, W. R., Anderson, B. E., Winstead, E. L., & Bagwell, D. R. (1998). Calibration and demonstration of a condensation nuclei counting system for airborne measurements of aircraft exhausted particles. *Atmospheric Environment*, *32*, 169–177.

Dorman, R. G. (1966). In C. N. Davies (Ed.), *Aerosol science* (p. 200). New York: Academic Press.

Freistas, M., Goncalves, H., Innocentini, M., Mullins, B., & Coury, J. (2006). Development of a double-layered ceramic filter for aerosol filtration at high temperatures: The filter collection efficiency. *Journal of Hazardous Materials*, *B136*, 747–756.

Heim, M., Mullins, B., Wild, M., Meyer, J., & Kasper, G. (2005). Filtration efficiency of aerosol particles below 20 nm. *Aerosol Science and Technology*, *39*, 782–789.

Heim, M., Mullins, B. J., & Kasper, G. (2006). Comment on: Penetration of ultrafine particles and ion clusters through wire screens by Ichitsubo et al. *Aerosol Science and Technology*, *40 144-145*.

Hemmer, G., Hoff, D., & Kasper, G. (2003). Thermoanalysis of fly ash and other particulate materials for predicting stable filtration of hot gases. *Advanced Powder Technology*, *14*, 631–655.

Hinds, W. C. (1999). *Aerosol technology*. New York: Wiley.

Ichitsubo, H., Hashimoto, T., Alonso, M., & Kousaka, Y. (1996). Penetration of ultrafine particles and ion clusters through wire screens. *Aerosol Science and Technology*, *24*, 119–127.

Kim, C. S., & Okuyama, K. (2006). Filtration efficiency of a fibrous filter for nanoparticles. *Journal of Nanoparticle Research*, *8*, 215–221.

Kim, S. C., Harrington, M. S., & Pui, D. Y. H. (2007). Experimental study of nanoparticles penetration through commercial filter media. *Journal of Nanoparticle Research*, *9*, 117–125.

Kirsch, A. A., & Stechkina, I. B. (1978). In D. T. Shaw (Ed.), *Fundamentals of aerosol science* (p.165) New York: Wiley.

Kreyling, W. G., Semmler, M., Erbe, F., Mayer, P., Takenaka, S., Schulz, H. et al. (2002). Translocation of ultrafine insoluble iridium particles from lung epithelium to extrapulmonary organs is size dependent but very low. *Journal of Toxicology and Environmental Health—Part A*, *65*, 1513–1530.

Lee, K. W., & Mukund, R. (2001). Filter collection. In: K. Willeke, & P. A. Baron (Eds.), *Aerosol measurement: Principles*, *techniques and applications*. New York: Wiley.

Mulholland, G. W., Henzel, V., & Babrauskas, V. (1989). The effect of scale on smoke emission. In: *Proceedings of the second international symposium on fire safety science*.

Oberdorster, G., Gelein, R. M., Ferin, J., & Weiss, B. (1995). Association of particulate air-pollution and acute mortality—involvement of ultrafine particles. *Inhalation Toxicology*, *7*, 111–124.

Scheibel, H. G., & Porstendorfer, J. (1983). Generation of monodisperse Ag- and NaCl-aerosols with particle diameters between 2 and 300 nm. *Journal of Aerosol Science*, *14*, 113–126.

Shin, W. G., Pui, D. Y. H., Fissan, H., Neumann, S., & Trampe, A. (2007). Calibration and numerical simulation of nanoparticle surface area monitor (TSI Model 3550 NSAM). *Journal of Nanoparticle Research*, *9*, 61–69.

Wang, H.-C., & Kasper, G. (1991). Filtration efficiency of nanometer-size aerosol particles. *Journal of Aerosol Science*, *22*, 31–41.

Wang, J., Chen, D. R., & Pui, D. Y. H. (2007). Modeling of filtration efficiency of nanoparticles in standard filter media. *Journal of Nanoparticle Research*, *9*, 109–115.

Willeke, K. (1976). Temperature dependence of particle slip in a gaseous medium. *Journal of Aerosol Science*, *7*, 381–387.

Yeh, H. C., & Liu, B. Y. H. (1974). Aerosol filtration by fibrous filters. *Journal of Aerosol Science*, *5*, 191–217.